frontiers | Frontiers in Earth Science

TYPE Original Research
PUBLISHED 22 July 2022
DOI 10.3389/feart.2022.804194

OPEN ACCESS

EDITED BY
Juliana Leme,
University of São Paulo, Brazil

REVIEWED BY
Francisca Martinez-Ruiz,
Spanish National Research Council (CSIC), Spain
Jeffrey M. Dick,
Central South University, China

*CORRESPONDENCE
Douglas Galante,
douglas.galante@lnls.br

SPECIALTY SECTION
This article was submitted to Paleontology, a section of the journal Frontiers in Earth Science

RECEIVED 29 October 2021
ACCEPTED 30 June 2022
PUBLISHED 22 July 2022

CITATION
Callefo F, Ricardi-Branco F, Alves Forancelli Pacheco ML, Cardoso AR, Noffke N, de Carvalho Teixeira V, Neckel IT, Maldanis L, Bullock E, Bower D, Moreira Silva A, Ferreira Sanchez D, Rodrigues F and Galante D (2022), Evidence for metabolic diversity in Meso-Neoproterozoic stromatolites (Vazante Group, Brazil). *Front. Earth Sci.* 10:804194. doi: 10.3389/feart.2022.804194

Evidence for metabolic diversity in Meso-Neoproterozoic stromatolites (Vazante Group, Brazil)

Flavia Callefo[1], Fresia Ricardi-Branco[2], Mírian Liza Alves Forancelli Pacheco[3], Alexandre Ribeiro Cardoso[2], Nora Noffke[4], Verônica de Carvalho Teixeira[1], Itamar Tomio Neckel[1], Lara Maldanis[5], Emma Bullock[6], Dina Bower[7,8], Adalene Moreira Silva[9], Dario Ferreira Sanchez[10], Fabio Rodrigues[11] and Douglas Galante[1]*

[1]Brazilian Synchrotron Light Laboratory, Brazilian Center for Research in Energy and Materials, Campinas, Brazil, [2]Department of Geology and Natural Resources, Institute of Geosciences, Universidade Estadual de Campinas (UNICAMP), Campinas, Brazil, [3]Laboratório de Estudos Paleobiológicos (LEPBio), Departamento de Biologia, Universidade Federal de São Carlos (UFSCar), Sorocaba, Brazil, [4]Department of Ocean, Earth and Atmospheric Sciences, Old Dominion University, Norfolk, VA, United States, [5]Université Grenoble Alpes, Université Savoie Mont Blanc, CNRS, IRD, Université Gustave Eiffel, ISTerre, Grenoble, France, [6]Earth and Planets Laboratory, Carnegie Institution for Science, Washington D.C., DC, United States, [7]Department of Astronomy, University of Maryland, College Park, MD, United States, [8]NASA Goddard Space Flight Center, Greenbelt, MD, United States, [9]Institute of Geosciences—University of Brasília, Brasília, Brazil, [10]Swiss Light Source (SLS), Paul Scherrer Institut (PSI), Villigen, Switzerland, [11]Department of Fundamental Chemistry, Institute of Chemistry, Universidade de São Paulo, São Paulo, Brazil

Deciphering the evolution of ecological interactions among the metabolic types during the early diversification of life on Earth is crucial for our understanding of the ancient biosphere. The stromatolites from the genus *Conophyton cylindricus* represent a datum for the Proterozoic (Meso to Neoproterozoic) on Earth. Their typical conical shape has been considered a result of a competition between microorganisms for space, light and nutrients. Well-preserved records of this genus from the "Paleontological Site of Cabeludo", Vazante Group, São Francisco Craton (Southern Brazil) present *in situ* fossilized biofilms, containing preserved carbonaceous matter. Petrographic and geochemical analyses revealed an alternation between mineral laminae (light grey laminae) and fossilized biofilms (dark grey laminae). The dark grey laminae comprise three different biofilms recording a stratified microstructure of microbial communities. These three biofilms composing the dark grey laminae tend to be organized in a specific pattern that repeats through the stromatolite vertical section. Iron and manganese are distributed differently along the dark and light grey laminae; X-ray absorption and luminescence data showed possible different areas with authigenic iron and iron provided from diagenetic infiltration. Cryptocrystalline apatite in the lowermost biofilms in each dark grey laminae may suggest past metabolic activity of sulfide-oxidizing bacteria. These findings suggest that the microorganisms reached a complex metabolic diversification in order to

maintain an equilibrium situation between the three different biofilms along the vertical section of the structures, thus benefiting the whole microbial community. This means that the stromatolites from the *Conophyton* genus may have formed as a result of a greater complexity of interactions between microorganisms, and not only from competition between photosynthesizers.

KEYWORDS

Conophyton, Proterozoic, microbial metabolism, sulfide-oxidizing bacteria, biomineral, biofilm

1 Introduction

Since the Archean microorganisms were able to adjust themselves to external factors by developing the ability of organization into a complex consortium of single or multiple species called a biofilm (Neu 1994; Neu 1996; Davey and O´Toole 2000). Biofilms are made up of secreted extracellular polymeric substances (EPS) that serve as protection for the cells, provide the exchange of metabolites, and work as a buffer against environmental factors, such as sudden changes in salinity, mechanical stresses, radiation and many others (Decho, 1999). By the trapping and binding of sedimentary particles and *in situ* mineral precipitation, the biofilms may construct organosedimentary structures called stromatolites (Hofmann, 1969; Walter, 1976; Burne and Moore, 1987; Riding, 2011; Noffke and Awramik, 2013). These are the result of biologically induced precipitation of minerals, especially carbonate, in a laminated form, whose process of mineral precipitation and bacterial growth is repeated until the structure grows vertically (Burne and Moore, 1987; Riding, 2011; Noffke and Awramik, 2013). These structures can follow different morphologies such as domical, stratiform, flat layered, columnar, branched, conical, among others, generally reflecting the environmental parameters in which the structure grew up (Hoffman, 1976; Walter, 1976; Grotzinger, 1989; Awramik, 1992; Hofmann, 2000; Zhang et al., 2021). However, conical stromatolites, such as those of the *Conophyton* and *Jacutophyton* genus, are known to reflect biological control in their morphology (Schopf, 1975; Bertrand-Sarfati and Moussine-Pouchkine, 1985; Kah et al., 2009). This means that its morphology results from the predominance of intrinsic factors (how the biota behaves and induces mineral precipitation) over extrinsic factors (how external parameters influence the shape of the structures, such as physical depositional factors as water currents and energy involved).

Stromatolitic structures of the *Conophyton* genus were generated in several locations around the world during the interval between the Meso and Neoproterozoic (approximately from 1.2 Ga to 900 Ma).Generally, they develop in specific conditions such as a marine subtidal environment, high water depth (up to tens of meters, but still within the photic zone) and low energy (without wave action, for example) (Moeri, 1972; Dardenne, 2000; Dardenne, 2005; Sallun Filho and Fairchild, 2005). These stromatolites have a characteristic morphology of a columnar structure without branches; in the vertical section, *Conophyton* is built up by conical laminae that were developed around a central axis (Sallun Filho and Fairchild, 2005). This type of stromatolite only occurs in between Meso to Neoproterozoic in records worldwide, although the reasons for this temporal restriction remain unknown. Therefore, *Conophyton* are considered a datum for this geological time interval (Preiss, 1976). There are several examples of *Conophyton* occurrence around the world, such as Vendian *Conophyton gaubitza* Krylov from Chichkan Formation (Karoy Group), South Kazakhstan (Schopf, 1976); Mesoproterozoic Atar Group, Mauritania (Bertrand-Sarfati, 1972; Bertrand-Sarfati and Moussine-Pouchkine, 1985; Kah et al., 2009; Burne, 2022); Mesoproterozoic in several units from Brazil: Paranoá, Itaiacoca, Bambuí and Vazante Group (Moeri, 1972; Cloud and Dardenne, 1973; Cloud and Moeri, 1973; Sallun Filho and Fairchild, 2005); Neoproterozoic *Conophytons* from Mina Verdun Group (El Calabozo Formation), Uruguay (Gaucher et al., 2004); Mesoproterozoic *Conophytons* from Helena Formation, Belt Supergroup, Montana, United States (Horodyski, 1985), among others.

It is hypothesized that the typical conical shape of *Conophyton* is a result of a competition for sunlight and space among microorganisms which formed the structures (Walter, 1977; Sallun Filho and Fairchild, 2005). The competition for sunlight and for nutrients in the same space would induce the biofilms to grow in greater volume towards the apical region of the stromatolite in formation. This is corroborated by the preservation of accumulated carbonaceous matter in the apical region of each laminae of fossilized stromatolites.

Stromatolites of subgroup *Conophyton cylindricus* Maslov 1937 are exposed at the "Paleontological Site of Cabeludo" belonging to the Sumidouro Member, Lagamar Formation, Upper Vazante Group, São Francisco Craton (Southeastern Brazil) (Moeri, 1972; Cloud and Moeri, 1973; Sallun Filho and Fairchild, 2005; Fairchild et al., 2015). These structures are remarkably well preserved despite their age of 1.350 Ma to 950 Ma (Cloud and Dardenne, 1973; Cloud and Moeri, 1973; Dardenne, 2005). Fossilized biofilms can be observed in its microscopic texture, intermingled with minerals. This opens a window for possibilities of exploration of possible biosignatures preserved in order to better understand the biological controls that exert a role in the conical formation.

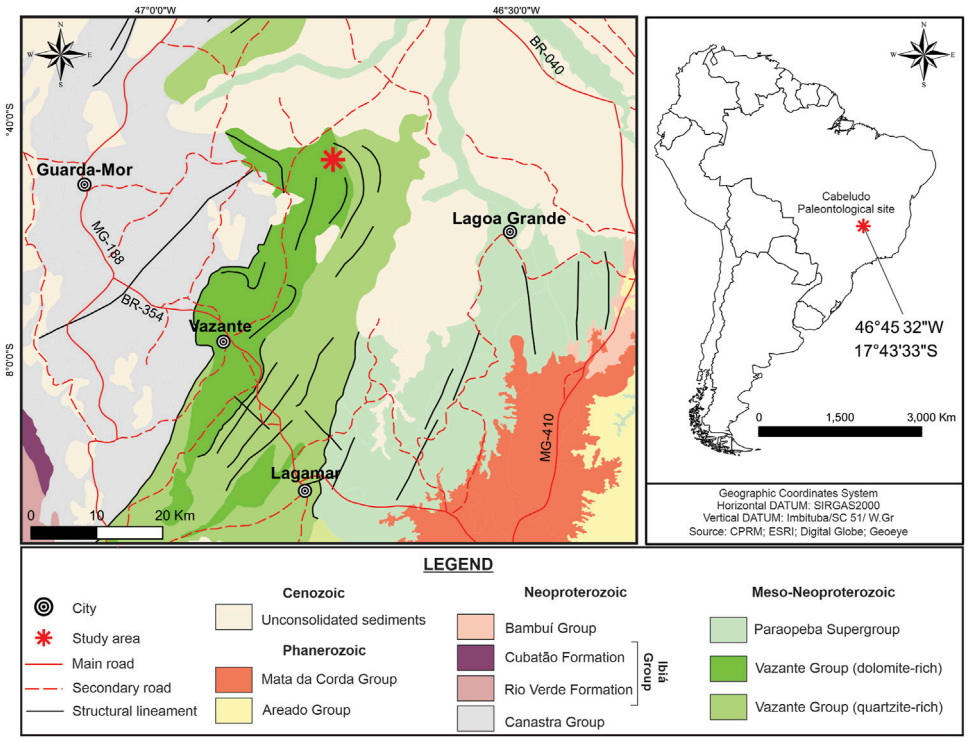

FIGURE 1
Geological map of Meso/Neoproterozoic Vazante Group, highlighting the Paleontological site of Cabeludo, in Vazante city (red star in the map), in Northwestern Minas Gerais State, Brazil (coordinates 17°43′ 33″ S; 46°45′ 32″W). The insert on the right indicates the location of the Paleontological site of Cabeludo in southeastern Brazil.

TABLE 1 Studied samples and applied techniques.

Sample	Macroscopic analysis	Petrology	EPMA imaging	Raman spectroscopy	XANES	XEOL	XRF	XRD
CP6/194	x	x						
CP6/195	x	x						
CP6/196	x	x	x	x	x	x	x	x
CP6/197	x	x						
CP6/198	x	x						
CP6/199	x	x						
CP6/200	x	x						
CP6/201	x	x						
CP6/202	x	x						
CP6/203a	x	x	x	x	x		x	
CP6/203b	x	x	x	x	x		x	

Petrographic thin-sections of the *Conophytons* from the Paleontological Site of Cabeludo revealed an alternation between dark-light laminated build-up composed mostly of amorphous silica (chert), quartz grains and dolomite, and dark-gray lamine composed of preserved organic matter (kerogen). These darker regions have been interpreted as

preserved biofilms (Dardenne, 2005). However, we observed a stratification within these preserved biofilms, which suggests a more complex construction of these stromatolites during the Meso-Neoproterozoic.

Here we propose the existence of more than one type of preserved biofilm in these *Conophytons*, besides an organization trend according to their metabolic needs responsive to environmental factors, similar to modern microbial mats. For that, we investigated the internal build-up of the ancient preserved biofilms in order to assess the development of the biofilm from its initial to mature stage. Our approach consisted of combining different methods at microscopic scales for understanding the microscopic textures and resolving the inorganic and organic phases. Petrographic analysis was used for preliminary inspection of the microscopic textures. Electron probe microanalysis (EPMA) provided us higher resolution information of the superficial textures, including the low Z elements present (e.g., C, O). For deeper investigation of the elements present at microns of depths and down to trace concentrations, we did synchrotron X-ray fluorescence (XRF) maps. Raman spectroscopy was used for mapping the presence of kerogen and some mineral phases, the last further corroborated by synchrotron-based X-ray diffraction (XRD). X-ray absorption (XANES) allowed us to deepen the chemical investigation by revealing the chemical species of Fe and Mn present in the samples, and X-ray excited optical luminescence (XEOL) added to this comprehension by providing maps of luminescent areas, signal of specific element valences. Together, these methods provided us with ways of deeper understanding of the geochemistry of the different *Conophyton* textures, and finding patterns that pointed to the presence of different metabolisms. These are represented by a differentiated geochemistry along the distinct preserved biofilms, which could mean biosignatures indicative of non-photosynthetic activities, and also biominerals resulting from the alternative metabolisms to photosynthesis, such as cryptocrystalline apatite (suggesting the past sulfide-oxidizing bacteria metabolic activity). The findings may indicate a greater complexity of microbial interactions between co-habitant microorganisms which formed the *Conophytons*, showing that these microorganisms developed other strategies of survival instead of competition by space and sunlight.

2 Geological setting

The orogenic belt of the Tocantins Province was formed by fusion of the Amazon Craton, the São Francisco Craton and the Paranapanema Craton (Dardenne, 2000), composing theGondwana supercontinent (Almeida, 1977). The Vazante Group is part of the Brasília Fold Belt, located in the west portion of the São Francisco Craton, and extended along approximately 250 km. It consists of low-grade metamorphic sequences of carbonates (dolomite) and pelites, whose deposition is attributed to a shallow marine platform setting (Falci et al., 2018). Late Mesoproterozoic age is indicated by the occurrence of conical stromatolites of the genus *Conophyton* in some stratigraphic units (Dardenne, 2000; Dardenne, 2005; Vasconcelos et al., 2020), and Re-Os dating that yielded 1,304 ± 210 Ma (Bertoni et al., 2014). Chronological constraints are established by U-Pb dating of detrital zircon grains from the Upper Vazante Group (Rocinha Formation), which provided 935 ± 14 Ma (Rodrigues et al., 2012). According to Dardenne (2000), the Vazante Group is stratigraphically divided into seven formations (from the bottom to the top): Retiro, Rocinha, Lagamar, Serra do Garrote, Serra do Poço Verde, Morro do Calcário and Serra da Lapa. The study site is located in the east portion of Lagamar Formation, which is subdivided in quartzite-dominated deposits (Arrependido Member) and carbonate-dominated deposits (Sumidouro Member). The Sumidouro Member consists of stromatolitic bioherm dolomites, breccias and dark gray limestones (Dardenne, 2000). Geographically, the fossil site is close to the city of Vazante, Minas Gerais State, in the southeast region of Brazil. The area was called "Paleontological Site of Cabeludo" in the description by Dardenne et al. (1972). The geographic coordinates are 17° 43′ 33″S and 46 °45′32 "W (Figure 1).

3 Material and methods

3.1 Field work

We collected eleven sets of samples of stromatolites from different points inside the paleontological site. Each one was taken from basal, middle, and top portions of the stromatolites, totalizing 33 samples. The samples are deposited in the paleontological collection of the Geosciences Institute, University of Campinas (IG - UNICAMP), receiving the denomination "CP" (paleontological collection) following the number of registry in the collection. Table 1 shows the samples and the method of investigation applied to each one. Those samples which presented better preservation of biofilms in thin section analysis were chosen to be explored with the techniques described subsequently.

3.2 Petrographic thin sections analysis

We prepared eleven thin sections of 30 μm thickness (without glass coverslip to allow compositional analysis). They were analyzed at the Paleohydrogeology Laboratory of the University of Campinas (UNICAMP), with a Carl Zeiss petrographic microscope Scope A1 ZEISS. The images were recorded with a ZEISS AxioCam camera and processed with ZEISS AxioVision® 4.8.2.0. (2006) software.

3.3 Electron probe microanalysis and energy dispersive spectroscopy

We obtained compositional analyses and secondary electron images using the JEOL 8530F electron probe at the Carnegie Institution for Science (Washington, DC). The images and maps were recorded in nine areas of interest within the CP6/196 thin section, sampling each putative kind of biofilm, besides areas of hydrothermal incursion, cracks and recrystallization areas. The probe was operated at 15 kV and 20 nA. We also performed quantitative analyses in each chosen point using the Thermo Scientific Energy Dispersive System (EDS), utilizing the Pathfinder software. Samples were coated with iridium to mitigate charging and to facilitate the analysis of carbon.

3.4 Raman spectroscopy

The Raman Spectroscopy analyses were performed at Carnegie Institution of Science (Washington, DC). The Raman images were acquired with the WITec Scanning Near-Field Optical Microscope, with a camera system coupled to the microscope. The excitation source was a frequency-doubled solid-state YAG laser (532 nm) operating between 0.01 and 5 mW output power. Spectra were collected on a Peltier-cooled Marconi 40-11 CCD chip, after passing through a f/4,300 mm focal length imaging spectrometer using a 600 lines/mm grating. We used the WITec Project Plus software to map peaks of interest across the sample and compute peak intensity maps.

3.5 Synchrotron-based μ-X-ray fluorescence and X-ray diffraction

Petrographic thin sections (30 μm thickness) mounted on glass slides were evaluated for their chemical and mineralogical composition using X-ray Fluorescence and X-ray diffraction. μ-XRF elemental maps were first acquired using the XRF beamline at the Brazilian Synchrotron Light Laboratory (LNLS), Brazil. The beamline was used in micro-beam mode with the KB focusing system in order to reach a beam size of 12 μm × 25 μm diameter. 2D measurements were performed at room temperature in continuous scan mode (fly scan), with step sizes of 30 μm and integrations of 300 ms per pixel. The excitation was made in white-beam mode. Further higher spatial resolution elemental maps were obtained at the microXAS beamline at the Swiss Light Source (SLS), Paul Scherrer Institut (PSI), Switzerland. The silicon drift detector (SDD) was placed at 70° with the incident beam in order to acquire the data, and the X-ray beam was focused down to 1 $\mu m^2 \times 1\ \mu m^2$ using KB mirrors. The measurements were carried out using a monochromatic beam at energy of 17.2 keV in order to excite the elements of interest. The step size was 30 μm for the overview area, and 3 μm for selected areas in the preserved biofilms, in order to acquire more details. All elemental maps were analysed using the PyMCA 4.6.0 software (developed by European Synchrotron Radiation Facility—ESRF, Solé et al., 2007).

The mineralogical composition was explored with X-ray diffraction in co-located measurements with X-ray fluorescence at the microXAS beamline. The measurements were made in three specific areas containing each type of biofilm separately. The angle between the X-ray beam and the sample was kept at $\Theta = 20°$ meanwhile the diffraction patterns were acquired using an area detector (Eiger 4 M) covering roughly $2\Theta = 35°$. The output data is composed of several 2D diffraction patterns where the presence of rings indicates a polycrystalline sample (Supplementary Figures S1A–C—top). To obtain the conventional Intensity vs. 2Θ diffractogram, an azimuthal integration was required and shown in Supplementary Figures S1A–C bottom. The main phases were identified using the software XRDUA (De Nolf et al., 2014).

3.6 X-ray absorption near edge structure

The micro XANES measurements were firstly performed using the XRF beamline (LNLS—UVX) around Fe K edge, and posteriorly using the Carnaúba beamline (LNLS - Sirius) around the Mn K edge. The XRF beamline was used in monochromatic beam mode, provided by the Si (111) crystal and a microbeam provided by the KB system (12 μm × 25 μm). Samples were measured in air and at room temperature, without sample-environment controls. The XANES spectra were collected in fluorescence mode, using the SDD detector available at the beamline (Ketek, GmbH). The higher spectral resolution was 0.3 eV. The Fe K-edge data from the sample was compared with synthetic standards (measured at the XAFS1 and XAFS2 beamlines of LNLS) and natural standards (measured with micro-beam in the XRF beamline). These mentioned studies were performed at LNLS UVX storage ring that is now decommissioned.

The Mn-K edges were also measured in the Carnaúba beamline (LNLS—Sirius), in order to have more accuracy in the obtained results, due to its resolution (beam size down to 150 nm × 400 nm, obtained with KB mirrors) and higher flux, once the new accelerator (Sirius) is a 4th generation machine and the beamline uses a 4-channel monochromator developed in-house (Tolentino et al., 2021). The measurements were acquired in fluorescence mode using Vortex®ME4 SSD detectors (Hitachi) on the energy range of 6,500–6,600 eV, with a step energy of 0.3 eV, accumulation time 0.5 s, in air and room temperature. The data was compared with that of synthetic standards of MnO (Mn^{2+}) and Mn_2O_3 (Mn^{3+}) measured in transmission mode with an Alibava (AS04-105A) photodiode.

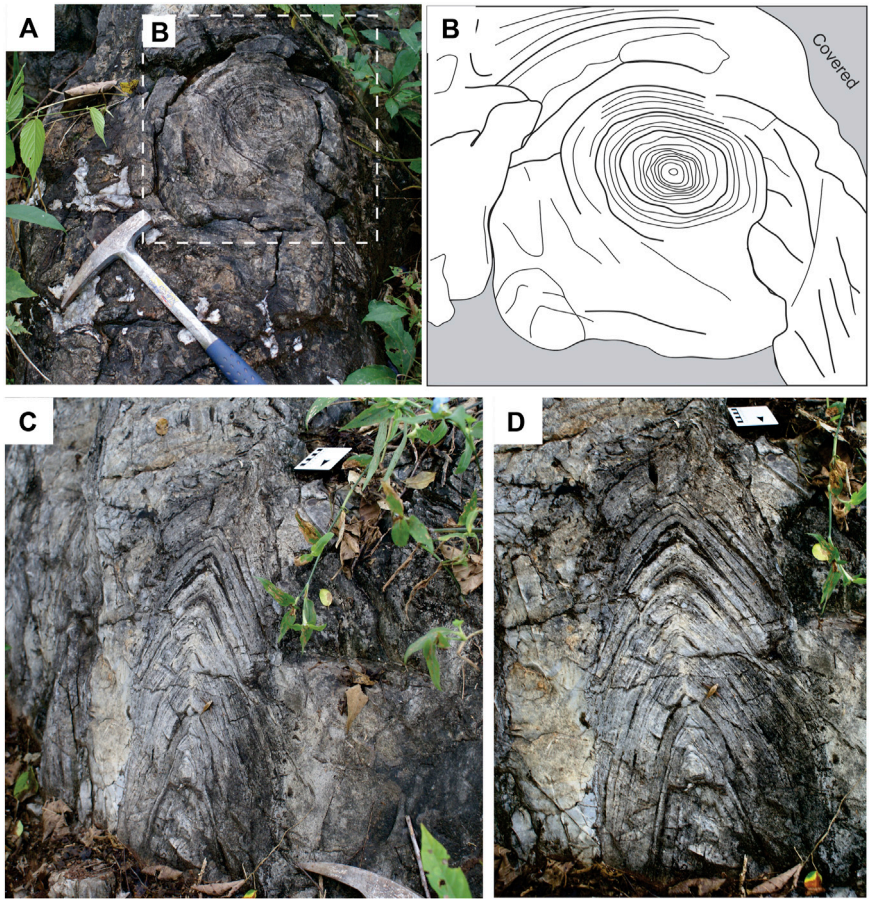

FIGURE 2
Morphology and internal build-up of *Conophyton* in outcrop; Paleontological Site of Cabeludo. **(A)** regularly-spaced concentric laminae in plan view (Scale: geological hammer—35 cm); **(B)** sketch of the concentric laminae, preservation degree increases toward the center of the structure; **(C)** conical laminae in profile view of the outcrop. Note closed angulation of the laminae and vertical alignment of the apex (Scale: 10 cm); **(D)** close-up view highlighting the planar contact between conical-shaped laminae and the host lithology (Scale: 10 cm).

3.7 X-ray excited optical luminescence

X-ray excited optical luminescence (XEOL) experiments were performed at the XRF beamline from the Brazilian Synchrotron Light Laboratory (LNLS), using the setup for microXEOL. This setup is composed of an Al-coated 15X objective reflexive lens (ThorLabs), with a working distance of 23 mm that is used to collect the light emitted by the sample after the interaction with X-rays. This light was collimated in a parabolic collimator (ThorLabs) also Al coated, and focalized in an optical fiber (UV-Vis, Ocean Optics) that was coupled to a spectrometer (QEPro, Ocean Optics). For exciting the samples, the white beam mode was used, with spot size of 12 μm × 25 μm. The optical signal was acquired in emission mode, with integration of 1s in each point, monitoring the range from 200–950 nm. The hyperspectral image was analyzed using the PyMCA software in 2D mapping.

4 Results

4.1 Morphology and internal build-up of the stromatolites

The stromatolites of the genus *Conophyton* at the Paleontological Site of Cabeludo occur as solitary units and arranged in clusters. The stromatolites range from 0.5 to 4 m high and are columnar in external morphology. As also observed by Sallun Filho and Fairchild (2005), the horizontal section through a stromatolite reveals its elliptical contour around the central axis, with diameters ranging from approximately 15–70 cm (Figures 2A,B). The conical laminae show high inheritance with each laminae presenting the same size, curvature and morphology of the previous laminae, as well apical areas of each lamination being well aligned to each other. As also pointed out by Moeri (1972), there is an

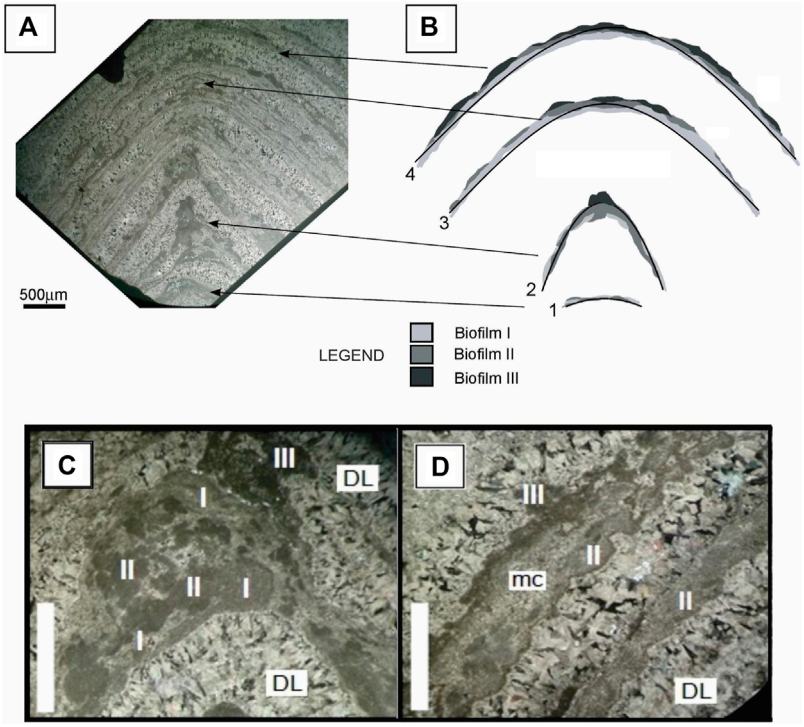

FIGURE 3
(A) Thin section overview showing alternating dark grey laminae and light grey to white laminae (scale bar: 500 µm); **(B)** sketch of the distribution pattern of the biofilms along four stages of development, forming the *Conophyton*'s organization; **(C)** Petrographic images of *Conophyton* showing three different organic-rich laminae. Cut in vertical section in the apical zone of organic-rich laminae of the *Conophyton* (scale bar: 500 µm), intermediate part of *Conophyton*; DL- dolomite; **(D)** cut in vertical section, top part of the *Conophyton*, lateral zone of organic-rich laminae (scale bar: 500 µm); DL—dolomite; mc - micrite. All images are from sample CP6/196.

elongation of the plan outlined in the stromatolites. In the vertical section from the base to the top, a vertical axis serves as support structure, and also present macroscopic layers, ranging from 0.5 to 1 cm. These stromatolites are conical-shaped with closed angulation in the bottom opening towards the top (Figures 2C,D). Whereas the apex of the young stromatolite was initially more conical (as recorded by the laminae close to the base), the apex increasingly became more pointed towards the top (Figures 2C,D). The angle of the laminae at the apex is 50° on average, but it can reach 30° in the basal laminae.

4.2 Microscopic texture in the stromatolites

We observed distinguishable alternations of dark grey laminae (400–600 µm thickness) and light grey to white laminae (700 µm–1 mm thickness) in petrographic analysis (Figure 3). Despite the overall good preservation of these *Conophyton* from the Vazante Group, post depositional modifications also occur, including mechanical compaction, ductile deformation (e.g., folding) and fractures filled with silica. However, these post depositional changes were not harmful to the evaluation of the original microscopic texture of the stromatolites.

The light grey to white laminae consist of rhombohedral coarse dolomite crystals with secondary recrystallization and scattered quartz grains, while the dark grey laminae consist of fine-grained dolomite crystals. In these laminae, organic matter was identified and preserved as brown-colored, opaque spots with no pleochroism. Rarely, dispersed fine-grained quartz grains occur. In close-up view, it is possible to observe that the dark grey laminae show three different organic-rich laminae, which were defined here as biofilm I, biofilm II and biofilm III (In Figure 3, shown as I, II and III, distributed in 4 stages of development of the *Conophyton*). The meaning of this division is explained in Section 5.2 of the discussions, as well as the division into the four stages of development of dark-grey laminae. The laminae differ in coloration from each other and they have a distinct mottled appearance related to varying carbon content. Notably, the vertical organization of the three different biofilms in each dark grey laminae is repetitive in all analyzed samples. The main visual aspect that differentiates the three biofilms is the

TABLE 2 Comparison of the main observed characteristics of the three biofilms comprising each dark grey laminae.

Biofilm	Color	Mineralogy	Crystal Size	Organic matter	Main elemental composition	Fe and Mn speciation
I	Darker grey	Dolomite, scattered quartz grains, apatite crystals	Fine-grained crystals	Diffusely distributed, high content, kerogen (D and G bands)	Ca, Fe, Mn, P	Fe^{2+} and Fe^{3+} Mn^{2+}
II	Intermediate grey	Dolomite, dispersed quartz grains	Fine-grained crystals	Diffusely distributed, high content, kerogen (D and G bands)	Ca, Fe, Mn, Sr, S	Fe^{2+} and Fe^{3+} Mn^{2+}
III	Lighter grey	Dolomite	Fine-grained crystals	Diffusely distributed, high content, kerogen (D and G bands)	Ca, Fe, Mn, Sr, S	Fe^{2+} and Fe^{3+} Mn^{2+}

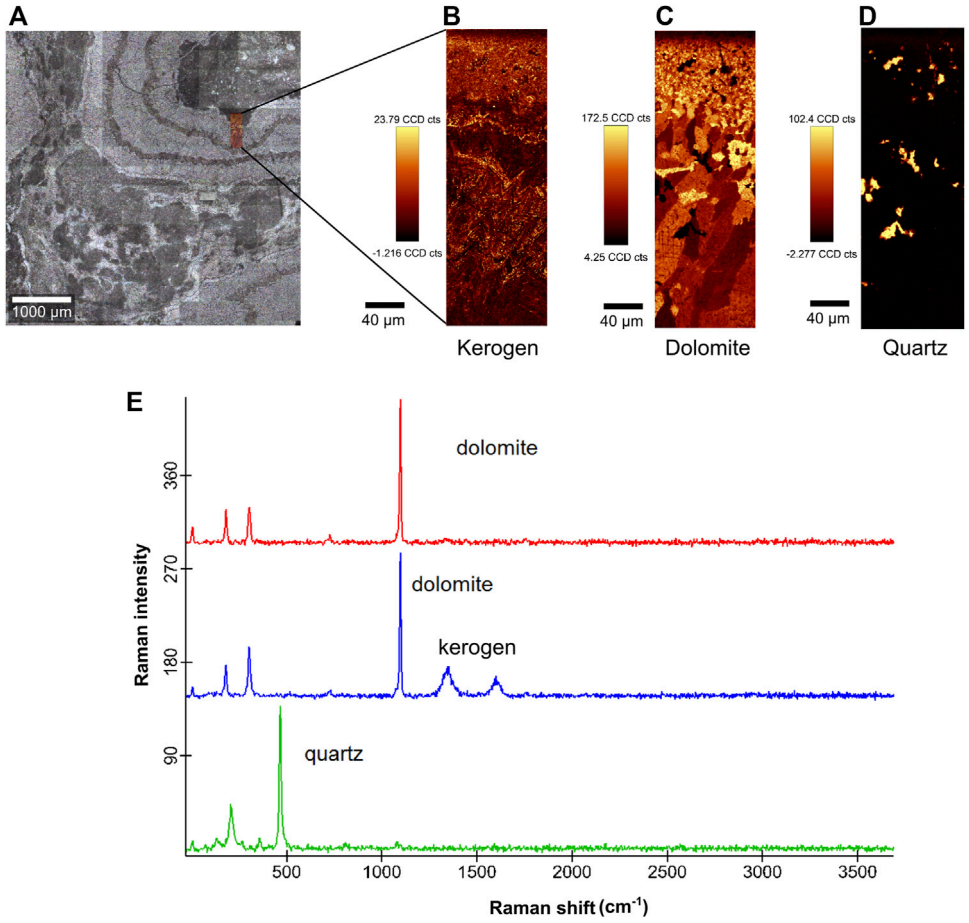

FIGURE 4
Raman spectroscopy analysis of the CP6/196 sample. **(A)** thin section with mapped area (0.2 mm × 0.6 mm), covering both dark grey laminae (biofilms) and light grey laminae (dolomite and quartz crystals); **(B)** map of quantitative distribution of kerogen showing higher counts for kerogen in the biofilm area; **(C)** map of quantitative distribution of dolomite showing homogeneous distribution in the two laminae; **(D)** sparse quartz grains distributed in both laminae; **(E)** Raman spectra of dolomite at 1,098 cm^{-1} (red and blue), carbon (kerogen) with D band at 1,366 cm^{-1} and G band at 1,583 cm^{-1} (blue) and quartz at 464 cm^{-1} and 203 cm^{-1}(green).

color, while the grain size and texture appear to be the same when looking at petrographic thin sections. However, the biofilm I showed exclusively microcrystalline apatite (Section 4.4), while the biofilm II and III showed highest intensity in fluorescence signal of Sr in comparison with biofilm I (Supplementary Figure S2). The Table 2 summarizes some main textural and

geochemical aspects which may be used to differentiate the three biofilms which comprises the dark grey laminae.

4.3 Petrological composition in Raman spectroscopy and X-ray diffraction

The Raman semi-quantitative peak intensity maps were acquired in an area covering both dark and light grey laminae (Figure 4A). The maps showed that in the biofilm area (dark grey laminae) had the highest counts of carbon (kerogen, D band—ca. 1,366 cm^{-1} and G band—ca. 1,583 cm^{-1}) in comparison with the light grey laminae (Figure 4B). Dolomite is the main component in light-grey lamine, except in areas with high counts of quartz (Figure 4C). The quartz is sparsely dispersed in the dark grey laminae and between the dolomite crystals in the light grey laminae (Figure 4D). Comparing the maps of quantitative distribution of kerogen (Figure 4B) and dolomite (Figure 4C), it is possible to observe that the kerogen is diffusely distributed between the microcrystalline dolomite in the dark-grey laminae, while in light-grey laminae, the kerogen is distributed near to the grain boundaries. The Raman spectra for each component are in Figure 4E: dolomite (1,098 cm^{-1}), kerogen (D band at 1,366 cm^{-1} and G band at 1,583 cm^{-1}) and quartz (464 cm^{-1} and 203 cm^{-1}).

The XRD data showed that the main mineral phase present in the Conophytons is dolomite. All Bragg reflexions (indexed according to the AMCSD 0000108, Graf 1961), correspond to dolomite (Supplementary Figure S1). However, the presence of discontinuous rings and isolated spots on the 2D diffraction patterns indicates that the beam is illuminating a small amount of crystallites. As a consequence, phases in a small fraction remain undetermined.

4.4 Petrology and composition using EPMA and EDS

In higher resolution analyses, the light grey/white laminae are composed of coarse components (approximately 100 μm–500 μm) including dolomite and scattered quartz grains. Dolomite commonly forms mosaics of euhedral to anhedral crystals, composing an idiotopic texture. The darker laminae are composed of microcrystalline dolomite with dissipated carbonaceous matter (ancient EPS and cell materials of the stromatolite). The apatite crystals measure from less than 1–10 μm (maximum). EDS and EPMA analysis show that the small crystals in the ancient biofilms (dark grey laminae; Figures 5A,B) are composed of Ca, Mg, C and O (Figure 5D), corroborating with the dolomite detected by Raman spectroscopy and XRD. Exclusively within the biofilms of the dark grey laminae (biofilm I) very small crystals composed of P, Ca, O and F (compatible with apatite ($Ca_5(PO_4)_3$—general formula) are distributed, Figure 5C.

4.5 Elemental composition of the textures in μ-XRF

Semi quantitative elemental maps with the spatial resolution of 30 μm were acquired in the surface area of 7 cm × 8 cm of the samples CP6/203a and CP6/203b (yellow square in Figures 6A,B). The maps were made covering all areas of interest (light and dark grey laminae, and region of hydrothermal vein) in order to compare the compositions. Ca is distributed all over the mapped area, related to dolomite crystals (Figures 6D,E). Si and K are present in some spots, the first one in spots containing authigenic quartz areas in light grey laminae. In the biofilm areas, the analyses showed the predominance of Ca and Fe (Figures 6D,E). The Mn is widespread all over the mapped area, but is present at higher concentration (intensity) in the region with hydrothermal veins, co-occurring with Fe (Figure 6D). Especially in the biofilm III area, Mn, Fe, S and Sr present in higher intensity than in the regions containing other biofilms (Figures 1, 6E, Supplementary Material). Signals from low Z elements such as Si, K and Al are more absorbed within the rock or by the air, making their detection harder than heavier elements. The lack of detection, therefore, does not imply the absence of these elements in our samples.

4.6 Chemical speciation of Fe and Mn contained in *Conophyton*

μ-XANES was applied to evaluate the Fe and Mn chemical speciation (Figure 7). Mn was also investigated with nano-XANES. Fe synthetic references based on iron oxides (Fe_3O_4, Fe_2O_3 and FeO), and Fe metallic (Fe^0) are compared to the *Conophyton* X-ray absorption spectrum, measured around the Fe K-edge. By qualitative analyses of the absorption spectra (Figure 7A) and the first derivative curves (Supplementary Figure S3), the results suggest Fe is present in a mix of 2+ and 3 + valences. Similar analysis was made to evaluate the Mn oxidizing state (Figure 7B). Even though the signal-to-noise is high due to the low concentration of Mn, it is clear, by qualitative analysis, the predominance of Mn^{2+}. It is noticeable that both measurements (biofilm I and II, and biofilm III) present edges position compatible with the one observed in MnO, which is a reference for Mn^{2+} indicating the predominance of Mn in 2 + form in both biofilms.

4.7 X-ray excited optical luminescence

The 2D map was made in an area of the *Conophyton* (sample CP6/196) covering the dark grey and light grey laminae and also the region containing a hydrothermal vein, in order to evaluate the difference in composition of original laminae and thermally modified areas (Figure 8A) through optical emission. The X-ray

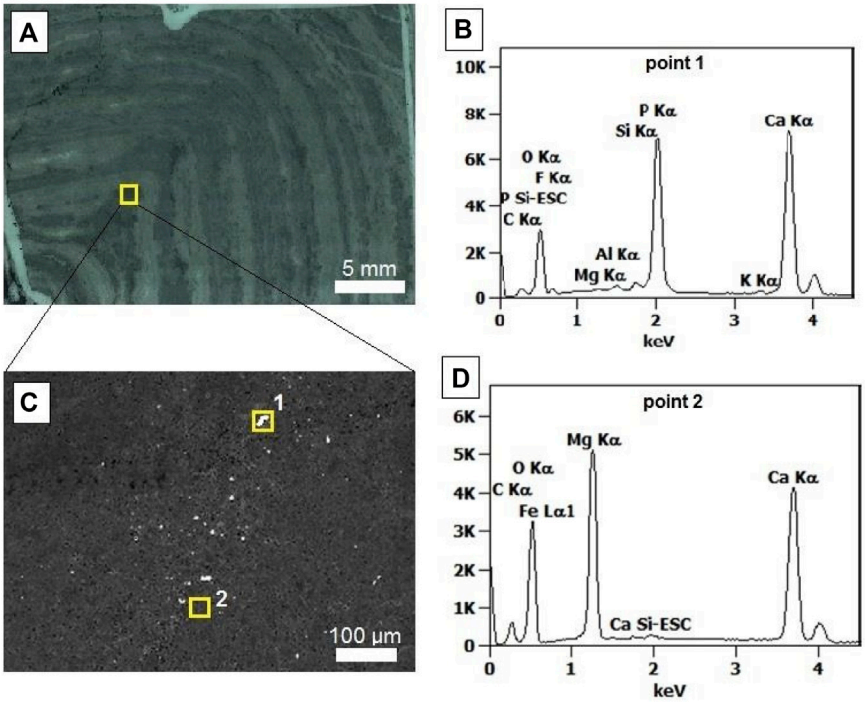

FIGURE 5
EDS spectra (sample CP6/196). **(A)** thin section showing the analyzed area (dark grey laminae, biofilm; indicated by square); **(B)** point 1 EDS spectra, compatible with apatite; **(C)** analyzed area with square 1 (mineral in biofilm II) and square 2 (matrix); **(D)** point 2 EDS spectra, indicating dolomite composition.

excited optical luminescence image (Figure 8B) shows the regions of more intense luminescence in the sample (yellow to red region, with corresponding general emission spectra with a broadband at the orange-red wavelength range at 650 nm). This area coincides with the diagenetic hydrothermal vein in *Conophyton*. Considering the co-location of Ca, Fe and Mn (XRF maps, Figure 6), the presence of dolomite (Raman—Figure 4; and XRD analysis—Supplementary Figure S1) and the presence of the chemical species showed in XANES analysis (Figure 7), the interpretation of the broadband in the general emission spectra (Figure 8C) leads to the conclusion that the Mn^{2+} within the dolomite lattice as the responsible for the luminescence emission.

5 Discussion

5.1 Preservation of biofilms

There is no evidence for bacterial cells and filaments preserved in the fossilized biofilms from the Conophytons of the Paleontological Site of Cabeludo. However, the biofilms are well preserved in both macro and microstructure. Here, we support that these biofilms have been partially preserved as organic matter (OM) diffused in a dolomitic matrix in regions considered to be authigenic (observed in petrographic thin sections as dark gray laminae) (Figure 3).

Contrary to what is assumed for the paleoenvironment of the stromatolites of the *Conophyton* genus, Moeri (1972) suggested a highly energetic subtidal basin as the most probable environment during the development of the *Conophyton* of the Cabeludo site. The main lines of evidences for the author's interpretation are 1) the great rate of carbonate supply and the early and rapid lithification required for the considerable height of the stromatolites; 2) the absence of subaerial exposure features (that explains the lack of signals of desiccation in the outcrop) which may exclude the possibility of supratidal or intertidal conditions; 3) the absence of micritic matrix; 4) the elongation of the plan outlines in most columns of the stromatolites, which may point to an influence of strong permanent water currents. According to Dardenne (2005), the early lithification was penecontemporaneous with dolomitization. Additionally, the sedimentary environment was described as a subtidal and deep marine setting, with the influence of sporadic tidal currents (that explains the existence of extremely dense bioherms isolated from each other, in addition to the deposition of micritic mud in the intercolumnar space, according Dardenne (2005).

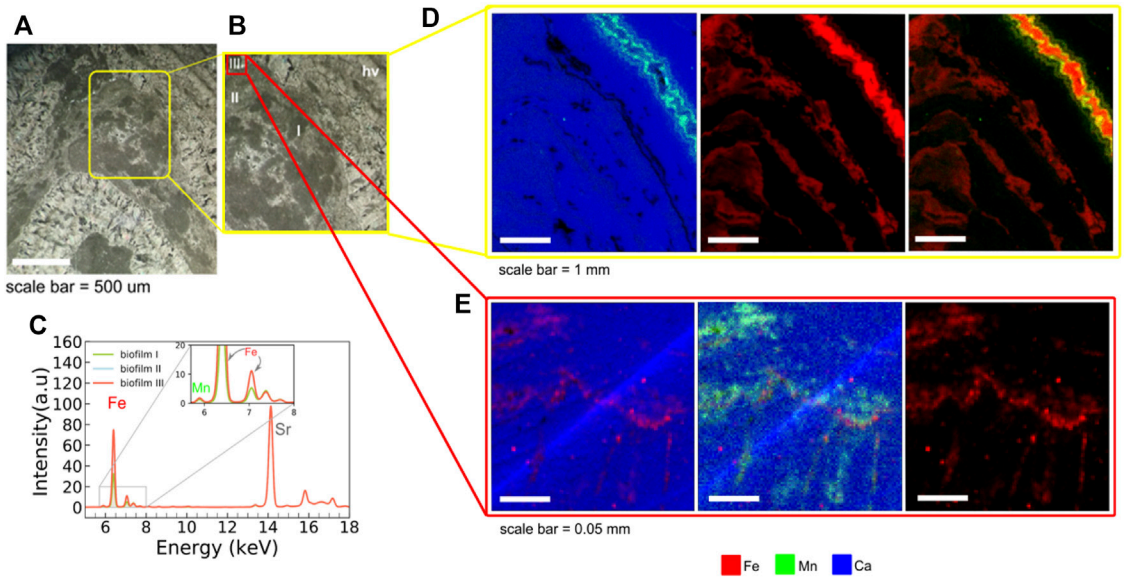

FIGURE 6
μ-X-Ray fluorescence elemental maps from the sample CP6/203b. **(A)** Petrographic image (scale bar = 500 μm) showing the area analyzed, containing the three types of biofilms (dark grey laminae) and light grey laminae. The yellow square represents the mapped area mapped with 30 μm step size; **(B)** Analyzed area (yellow square) with biofilm I, II and III and hydrothermal vein (hv) mapped in 30 μm stepsize (LNLS) and area of biofilm III selected to be mapped with higher resolution at microXAS beamline, SLS (red square); **(C)** X-ray fluorescence spectra of Fe, Mn and Sr, obtained in the mapped areas from biofilm I, II and III; **(D)** elemental maps with 30 μm of step size (XRF beamline, LNLS) in area covering the three types of biofilms, plus an area with hydrothermal vein (with highest intensity of Mn), scale bar = 1 mm; **(E)** elemental maps with 3 μm of step size (microXAS beamline, SLS) of area covering the biofilm III. All maps of the figure show the composition of Ca (blue), Mn (green) and Fe (red).

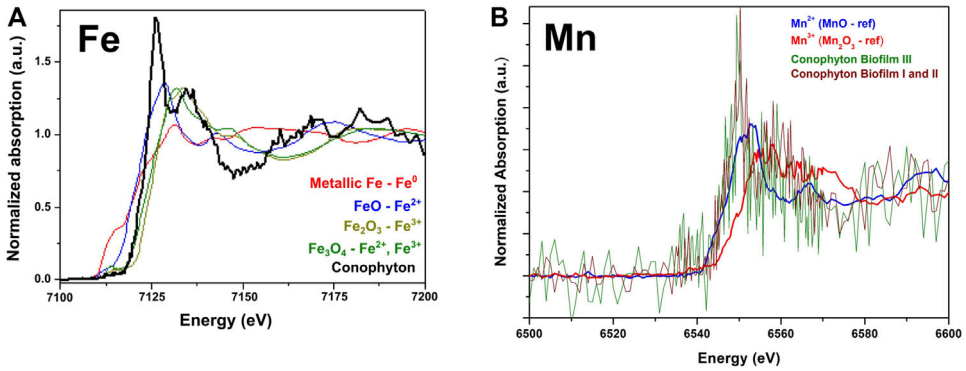

FIGURE 7
XANES absorption spectra of the sample CP6/196. **(A)** Normalized absorption curves and comparison between the synthetic Fe standards and the *Conophyton* sample; **(B)** Normalized absorption curves of synthetic Mn standards and *Conophyton* sample.

The early and rapid lithification plus the high rate of sedimentation may have prevented and/or delayed the degradation of the biofilms by aerobic microorganisms. In fact, Raman data acquired in this study shows the preservation of OM, as evidenced by the D and G bands (1,366 and 1,583 cm^{-1}) of kerogen. The quantitative maps (Figures 4B,C) show that kerogen is distributed in a diffuse way in the dark-gray lamine, while in the light-grey laminae it is limited to the grain boundaries. This can means that in the dark-grey laminae the OM could be preserved *in situ*, even with the post-diagenetic events. In contrast, in the light-grey laminae, the kerogen was moved to the grain boundaries or in between regions of overgrowth of grains (Figure 4B) due to the secondary dolomitization. The dolomitization can make the preservation of

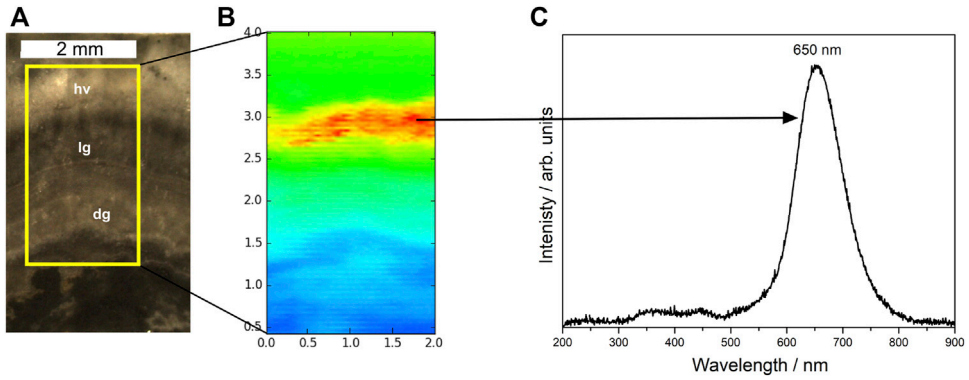

FIGURE 8
X-ray excited optical luminescence (XEOL) image with respective emission spectra under X-ray irradiation. **(A)** Selected area to be mapped (scale bar: 2 mm), covering areas with dark (biofilms, dg) and light grey laminae (lg), and region with hydrothermal vein (hv); **(B)** X-ray excited optical luminescence (XEOL) temperature scale image (2 mm × 4 mm), acquired at the X-ray Fluorescence (XRF) beamline at the LNLS with step size of 30 μm; **(C)** general emission spectra showing a broadband at the orange-red wavelength range at 650 nm.

the microbial morphology difficult (Bartley et al., 2000), but OM can be preserved even after secondary dolomitization, mainly as organic matter particles trapped within dolomite crystals (Murphy et al., 2020).

This sedimentological context also supports a mineral-associated organic matter (MAOM) hypothesis. By studying different types of carbonates of microbial origin in different environmental contexts, Melim et al. (2016) indicated that the entombment of microbes and EPS in carbonates is more widespread than previously thought: it does not occur in travertines, for example, because of the photolytic degradation by sunlight, elevated temperatures, and aerobic microbial degradation. Hence, considering the environmental and physical conditions mentioned for the good preservation of the microbial signatures mentioned above, the paleoenvironmental context of Conophytons from the Cabeludo could have favored biofilm preservation due to the fast mineralization.

As observed in XRF elemental maps (Figure 6), it is remarkable that iron is co-located exclusively with the biofilm preserved laminae and in some post-diagenetic features, such as fractures with incursion of hydrothermal fluids. Mineral-associated organic matter (MAOM) in sediments is commonly adsorbed or co-precipitated with the iron minerals (Lalonde et al., 2012). MAOM is thought to persist because OM can form strong chemical bonds to minerals and can be physically protected in microaggregates or co-precipitates (Kögel-Knabner et al., 2008). The association of OM with minerals can restrict the diffusion of oxygen, slowing down natural degradation and protecting it from decomposers. According to our XANES data there is a mix of valencies of iron in the biofilm preserved laminae of *Conophyton*, consisting of Fe^{2+} and Fe^{3+}. The Fe^{3+}, exerting a structural role, may serve as a connective cement allowing the formation of aggregates of OM and minerals. Also, the Fe^{3+} may serve as a sorbent in which the OM adsorb or co-precipitate with the Fe^{3+} minerals (Chen et al., 2020). In this sense, the Fe^{3+} detected in the region of preserved biofilms may also have been another factor that helped the preservation of OM in Conophytons.

5.2 Distribution of different biofilms inside the *Conophyton*

Modern microbial mats can be considered relevant analogues to understand the ecology and the formation of stromatolites, (Dupraz et al., 2009; Foster and Mobberley, 2010; Saghai et al., 2017). The microbiota of a well-developed and stratified microbial mat is very diverse (Des Marais, 1990), composed of microorganisms that form a biogeochemical gradient according to the metabolic needs of their functional groups (Dupraz and Visscher, 2005; Dupraz et al., 2009).

In fact, even in Archean time, microbial mats could already exhibit structural and biological complexity in their ecosystems (Nisbet and Fowler, 1999). Hickman-Lewis et al. (2020) showed evidence of coexistence between Bacteria and Archaea on microbial mats dated 3.5–3.3 Ga based on fossilized biopolymers detected by Fourier transform infrared spectroscopy (FTIR). The microbially induced sedimentary structures (MISS) in the 3.48 Ga Dresser Formation record that benthic microorganisms could already assemble biofilm communities to biofilm forming geomorphologically controlled catenae in response to environmental conditions (Noffke et al., 2013). The more different kinds of microorganisms compose a biofilm, the more complex its internal build-up becomes. Biofilm development integrates

growth conditions and the microbial composition in such a way that the available resources have an optimal exploitation (Tolker-Nielsen and Molin, 2000). An early stage of biofilm includes few microbial groups and a simple internal build-up (often just a few layers); a more mature biofilm, however, has a higher degree of organization and may show a mottled structure (Stoodley et al., 2002; Stolyar et al., 2007; Pernthaler et al., 2008).

Stromatolites are formed initially by microorganisms in a microbial mat and their metabolic activity and geochemistry leads to induction of calcium carbonate precipitation (Reid and MacIntyre, 2000; Dupraz et al., 2009). But not all microbial mats develop a stromatolite; it depends on the microbiota composition, the dominant metabolisms and the surrounding geochemical environment (Havemann and Foster, 2008; Foster and Green, 2011). Stromatolites, in general, are formed mainly by photosynthesizing microorganisms, especially filamentous cyanobacteria (Awramik and Margulis, 1974; Burne and Moore, 1987; Riding, 2011; Noffke and Awramik, 2013), but its microbial diversity may be greater, depending on the environmental parameters. Foster and Green (2011), in an experiment with cultivation-independent molecular techniques in several modern stromatolites, attested to a greater microbial diversity in marine and hypersaline stromatolites. Based on the complexity of the ecosystems that gave rise to some of the stromatolites and microbial mats in the Precambrian, comparing them with their modern representatives, and based on the evidence showed here, we suggest the possibility of greater complexity in the formation of Conophytons from the Paleontological Site of Cabeludo.

According to Walter (1977) and also Sallun Filho and Fairchild (2005), the conical shape typical of *Conophyton* denotes the competition for space, nutrients, and light between microorganisms. This would cause an accumulation of biomass at the apex of the forming stromatolitic structure, resulting in the conical shape observed in the microbialites of the genus. However, in this study, the textures on the analysed thin sections point to the existence of different types of biofilms preserved in each dark grey laminae of the stromatolites at the Cabeludo Paleontological Site, revealing at least three communities or populations of microorganisms (distinct or not) growing at the same time. It may imply more than one metabolic group forming the structures, rather than only photosynthesizers competing for sunlight. These three different types of biofilm show a clear tendency to organize into a specific repetitive laminae pattern revealing sequence and cyclicity observed in thin sections across the longitudinal axis of several samples of *Conophyton*. Figure 9 schematizes the evolution of spatial distribution and organization of the three types of biofilms (here called biofilm I, II and III) over the time; the evolution takes place in four stages (denoted in the yellow squares in Figure 9):

Stage 1: in the initial phase of the stromatolite formation, the biofilm I and II were formed. The biofilm I is located in the deeper zone of the mat, while the biofilm II is located in the surface; this arrangement may be due to affinity (synergy) and similar needs of the two constituents for resources such as nutrients and light.

Stage 2: a new type of biofilm (biofilm III) colonizes the preceding two biofilms. It is positioned above the biofilm II, demonstrating a certain competition among the different species for light. This can be observed by the higher concentration of biomass (II and III) starting to accumulate at the apex of the laminae. At this stage, biofilms I and II appear to be distributed in the same pattern observed in stage I, while the biofilm III occupies the upper zone near the apex of the laminations.

Stage 3: the three biofilms appear to have reached a certain equilibrium regarding their spatial distribution and organization according to each metabolic needs: an even pattern of distribution of the biofilms is established, following the sequence of development (from the bottom to the top of the community): biofilm I → biofilm II → biofilm III.

Stage 4: the pattern of spatial distribution and organization of the biofilms reached in the stage 3 starts to repeat until the top of the stromatolites, as observed in thin sections of the top part of the structures.

5.3 Depositional versus post-depositional processes: Origin of internal organization of *Conophyton*

Along the Conophyton, laminae with a pointed apex (especially those formed by greater mass of biofilms) may show high competition between constituents. Where the stromatolite apex is more rounded, the biofilms have been assembled and reached an equilibrium stage, which is stage 4. A possible interpretation for the difference in biofilms distribution is that, at certain times of high environmental stress (such as decrease of nutrient availability), probably due to a periodic lack of illumination, the biofilms' community disperses and moves towards the best light and nutrient exposure regions. The competition for the resources is documented by biofilm in stage 2. The stage 1 is the original state of distribution of biofilms (types I and II) in the beginning of the microorganism proliferation; due to a possible increase in light and nutrient provision, the biofilm type III started to associate with the original biofilms I and II. Possibly motivated by environmental stress, biofilm III struggled towards the top after spreading out, establishing an equilibrium situation, which was maintained until the top of the structures. Our most plausible hypothesis to explain this interaction and distribution between biofilms I, II and III is that at least the biofilm II and III were constituted by photoautotrophs. In contrast, the biofilm I, which preferentially remains at the base of the stratification

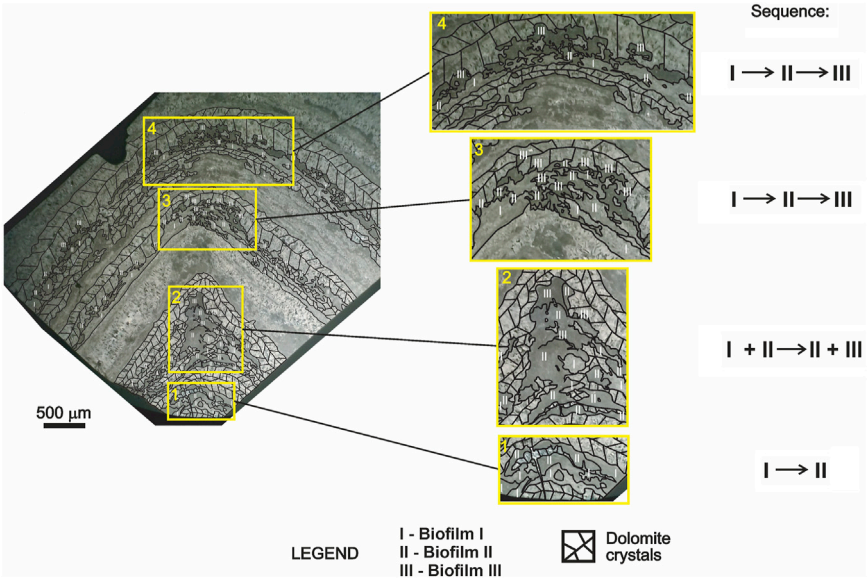

FIGURE 9
Distribution of the three different biofilms in *Conophyton* from the bottom to the top of a thin section (CP6/203b). Sequence of distribution of the different biofilms from the bottom of the structure (stage 1; 1 in yellow square) to the upper laminations towards the top (stage 4; 4 in yellow square) and organization of the biofilms according to resources. In stage 1, the biofilm II is organized above the biofilm I. In stage 2 (2 in yellow square), a new type of biofilm (biofilm III) develops above the biofilm I and II, in the apex of the dark grey laminae. In this stage, the biofilm I and II remain diffusely organized (represented by I + II), while the biofilm III is arranged at the apex, but still seems to mix with the biofilm II (represented by II + III). In the next stage (stage 3 and 4), the sequence of distribution follows the pattern (from the bottom to the top of the laminae: biofilm I → biofilm II → biofilm III.) The pattern is repeated in the subsequent laminations to the top of the stromatolite.

formed, possibly belongs to a non-photosynthetic metabolic type. However, in situations of environmental stress due to the lack of nutrients and sunlight, biofilm III would be more effective than biofilm II, reaching the top to ensure its survival.

Other hypotheses include the influence of textural aspects (crystal size, porosity and permeability) that likely might have controlled the distribution of the organic matter within the rock framework. The repetitive organization of biofilms and their vertical distribution indicates that textural aspects did not exert a major influence in organic matter content. If this was the case, a random distribution of kerogen would be expected. Similarly, heterogeneous modifications by weathering are not the case, since oxidation and chemical reactions would cause degradation of the organic matter from the top toward the bottom, which is not the case in the Cabeludo site. In addition, weathering would damage the internal organization of the *Conophyton* structure. Lastly, although metamorphism and hydrothermalism occur in the vicinity of the study area, some criteria (e.g., preservation of original structures, lack of high temperature/high pressure minerals) indicate that these processes did not cause significant modifications in the composition of the *Conophyton*. Geochemical data exhibit predominance of Ca, Fe and Mn, whereas elements commonly associated with high temperatures (Cu, Pd, Zn) were not detected in the analyzed samples. The only signal of hydrothermalism affecting the Cabeludo site is fracture-filling veins, but this process likely took place after lithification, as indicated by the predominantly tabular-shaped veinlets that crosscut the *Conophyton*. Metamorphic evidence is not present in the study area, since the recrystallization of dolomite is interpreted to have occurred during diagenesis.

5.4 Geochemical evidence and possible biosignatures for the biofilm differentiation

Exclusively in areas with biofilm I (and sometimes in the biofilm II), phosphate occurs as cryptocrystalline apatite. As shown in Figure 5D very small crystals of apatite appear in the biofilm II area (within the dark grey laminae) while in the other areas, such as the biofilm III and the light grey laminae, the phosphate mineral was not found. As observed, the biofilm I preferentially remains at the base of the stratification in each dark grey laminae, meaning a lower need for sunlight than biofilms II and III. Therefore, there is a possibility that biofilm I may consist of non-photosynthetic species.

Caird et al. (2017), studying Ediacaran stromatolites from Salitre Formation, Brazil, reported the occurrence of phosphorites (francolite) in microbial laminae, whereas strontian fluorapatite occurs between stromatolitic layers. They interpret the accumulation of phosphorites as a consequence of the activity of chemosynthetic bacteria, which, benefiting from the redox gradient caused by the production of photosynthetic oxygen,

promote the *in situ* precipitation of phosphorites. The XRF data in this study showed the presence of Sr in both biofilms I, II and II, but the highest intensity was observed in the biofilm III mapped area. However, we could not identify the link between Sr with the phosphorites in at least the biofilm I and II (in which the phosphorites were found). The Sr is co-located with Ca in some regions in biofilm II and III (Supplementary Figure S2), but it is common the incorporation of metals, such as the strontium (Sr^{2+}, VI-fold coordination, Ionic radius: 1.18 A), into the $CaCO_3$ mineral phases, when the metals replace the calcium (Ca^{2+}, VI-fold coordination, Ionic radius: 1.00 A) in the crystal lattice. As a consequence, there is a co-precipitation of the solid formed, such as the $SrCO_3$, or even a calcite doped with Sr^{2+}. Ferris et al. (1995) showed that the incorporation of Sr-rich groundwater during the microbial calcite nucleation promoted the solid solution of $SrCO_3$ in calcite. In Conophyton, it is possible that Sr may have been associated with the microbially-induced calcite nucleation during the growth of the stromatolite, explaining the co-location of Ca and Sr in the fossilized biofilm zones. However, it is not possible to exclude the hypothesis of substitution of Ca^{2+} by Sr^{2+} in the crystal lattice of carbonates by abiotic way.

Although the formation of phosphatic minerals in marine environments is still poorly understood, the involvement of bacteria in this process is presumed. Dissolved phosphorus in the ocean water is easily incorporated by photosynthetic organisms (Compton et al., 2000). However, organic matter can capture the phosphorus and remobilize it by microbiological processes. Crosby and Bailey (2012) discussed the role of microorganisms in the genesis of phosphatic minerals using several works to exemplify the relationship of microorganisms with different mediation mechanisms in apatite formation. One of them was proposed by Schulz and Schulz (2005), in which the vacuolated sulfide-oxidizing bacteria (SOB) can concentrate polyphosphates in pore water, where apatite is constantly precipitating. According to Crosby and Bailey (2012), several factors may have an effect on the rate of precipitation of apatite, such as the pH, redox potential, the existence of suitable nucleation sites, activation energy for the precipitation, and the microbial activity may influence all of them. Williams and Reimers (1993) and Williams (1984) documented a relation between bacteria and phosphorite formation in fossil record. In their study, they suggest that SOB were involved in phosphogenesis in fossil microbial mats with phosphate-rich laminations under aphotic conditions. In Conophytons, the fact that biofilm I is located in the deepest layer of dark-grey laminae exposes it to constant sunlight deprivation, since photosynthetic biofilms are always above them.

Shukla et al. (2020) described the influence of SOB in the formation of phosphorites in association with biofilms preserved in Neoproterozoic shales. They argue that bacteria, in an extracellular way, create redox conditions favorable to the precipitation of phosphorites. In that case, the bacterial EPS or the chemical ligands in the cell wall provide nucleation sites and decrease the activation energy for the mineral precipitation. A similar situation may have occurred in the biofilm zones I (and even II) of the Conophytons. The phosphate precipitation is favored due to the acidification of the medium when the oxygen serves as an electron acceptor in the SOB cell walls (Crosby and Bailey, 2012). The inorganic phosphate precipitation could be considered in Conophytons, however, the mineral occur only in areas of biofilm I and sometimes, II, never occuring in the biofilm III laminae. Another evidence for the exclusion of this possibility is the size of the crystals, never reaching more than 10 μm.

The XRF maps show that the region of preserved biofilms in *Conophyton* is rich in Ca, Fe and Mn (Figure 6). In these areas, Ca is co-located with Fe and Mn (the latter one with low intensity), while in the diagenetic hydrothermal vein, the Ca is co-located with Fe and Mn (with higher intensity than in fossilized biofilm areas). The Raman spectra (Figure 4) and XRD analysis (Supplementary Figure S1) showed the presence of dolomite in both areas. Mn^{2+} is known to induce high luminescence intensity in dolomite even in ppm concentration (i.e., as a trace element), and its emission is represented by a broadband at the orange-red region with maximum wavelength *ca.* 650 nm (Figure 8C), while the Fe^{3+} works as a luminescence quencher (Pierson, 1981; Marfunin, 1995; Habermann et al., 1998). In the XEOL emission spectra (Figure 8C), it is observed as a broadband that is ascribed as the 3d5 → 3d5 4T1(4G) → 6A1(6S) Mn^{2+} (Marfunin, 1995; Shionoya et al., 2007; MacRae and Wilson, 2008; Gaft et al., 2015). In the XEOL emission spectra (Figure 8C) it is observed as a broadband in the orange to red region in the electromagnetic spectrum, which is ascribed as the typical 3 d^5 → 3 d^5 $^4T_1(^4G)$ → $^6A_1(^6S)$ Mn^{2+}. This is a characteristic electronic transition from this ion that describes the decay from an excited energy level 4T1 (4G) to the ground level 6A1(6S) This result indicates that the hydrothermal vein, the region of the most intense luminescence (Figure 8B) is rich in dolomite doped with Mn^{2+}, diagenetically included after the lithification of the stromatolitic structure. Additionally, the X-ray absorption analysis detected the presence of chemical species such as Fe^{2+}, Fe^{3+} in areas of preserved biofilms. The Fe^{3+} are present in hydrothermal veins and cracks, possibly the result of diagenetic incorporation by incursion of hydrothermal fluids and/or groundwater before the stromatolite's lithification.

The decomposition of OM during the early diagenesis by the action of microorganisms from the biofilm itself can produce humic substances, a complex mixture of organic components synthesized during the decomposition of matter original OM (Lovley et al., 1996). This can also be caused by the burial of biofilms due to the mineral precipitation process during the growth of the stromatolitic structure. Once stable, the humic substance can serve as electron donors for other microorganisms, which use them in their energy generation processes (for example, *Geobacter metallireducens* to reduce ferric iron—Fe^{3+}). The reduction of Fe^{3+} is then conducted abiotically, reoxidizing the humic substances previously produced (Lovley et al., 1996). In *Conophyton*, the iron is

widespread over the biofilm-preserved laminae and in fractures filled diagenetically by fluids. The Fe^{2+} is diffusely distributed in regions of biofilm preservation, possibly being interpreted as a product of abiotic reduction of Fe^{3+} and/or product of the reduction of Fe^{3+} through the action of iron bacteria as electron acceptors from the biotic decomposition of organic matter. The role of iron in microbial ecosystem is diverse: (I) it allows the electron transfer in the system (the Fe^{3+} accept electrons from microbes or Fe^{2+} donate electrons for oxidants); (II) it serves as a sorbent in which the OM absorb Fe^{3+} in minerals, and (III) the Fe^{3+} can serves as connective cement binding OM and minerals (Chen et al., 2020). This last role is what probably happened during the fossilization process of the biofilms in Conophytons of Cabeludo Paleontological Site.

6 Conclusion

The stromatolites of the subgroup *Conophyton cylindricus* Maslov present in the Paleontological Site of Cabeludo, Vazante Group in Brazil, are a typical occurrence of the conical bioconstructions from the Mesoproterozoic. These structures present, at the microscale, morphological characteristics pointing towards the past presence of a stratification of at least three different types of biofilms forming the preserved organic laminae (the dark grey laminae) of the stromatolite. The three different biofilms form a pattern of distribution denoting an equilibrium situation between them towards the top of the structures. The presence of carbonate laminations rich in phosphates in the deepest biofilms in each dark grey laminae (biofilms I and II) are indicative of the possibility of past existence of sulfide-oxidizing bacteria. Thus, the diversity in the microbiota which formed these stromatolites was greater than previously thought, explaining the microscopically observed stratification.

Data availability statement

The datasets presented in this study can be found in online repositories. The names of the repository/repositories and accession number(s) can be found in the article/ Supplementary Material.

Author contributions

All the authors contributed in the writhing, interpretations and discussion of the results. FC, F-RB and AM made the field trip for collecting samples; VC, IN, DG, LM, EB, NN, DB and DF participated of the sample's analysis, processing data and interpretation; MA, AR, NN, VC and F-RB participated in the discussion of results; F-RB coordinated the first phase of the study and provided the financial support for the field trip.

Funding

Brazilian Federal Agency for Support and Evaluation of Graduate Education—CAPES and the PDSE Program for the financial support, and scholarship in the beginning of the study; National Council for Scientific and Technological Development—CNPq Research Productivity Grants (310817/2020-0, 310,890/2021-7 and 303527/2017–0) and the São Paulo Research Foundation—FAPESP grants 2016/20927-0 and 2016/06114-6 (for funding the field trips to collect the samples), 2020/02537-5 and 2021/05083-8 for funding analysis and fellowship for this project, and 2015/21810-6 scholarship; the French National Research Agency in the framework of the Investissements d'Avenir program (ANR-15IDEX-02).

Acknowledgments

The authors thank the University of Brasília, Nexa Resources and the geologist Bruno Baptistella for the support in the field trip; the Brazilian Synchrotron Light Laboratory (LNLS) for the facilities (μ-XRF, μ-XEOL, and XANES, proposals 20150076, 20160140 and 20180687) and Carnauba beamline (XANES, proposal 20210014); the microXAS beamline at Swiss Light Source (SLS, proposal 20190823); the Earth and Planets Laboratory at the Carnegie Institution of Science (Washington, DC) for the availability of the Raman spectrometer and EPMA microprobe. We also thank Dr. Silvio Y. Onary Alves (USP) for some clarification on terms and concepts about biological evolution.

Conflict of interest

The authors declare that the research was conducted in the absence of any commercial or financial relationships that could be construed as a potential conflict of interest.

Publisher's note

Supplementary material

The Supplementary Material for this article can be found online at: https://www.frontiersin.org/articles/10.3389/feart.2022.804194/full#supplementary-material

References

Almeida, F. F. M. (1977). O cráton do São Francisco. *Rev. Bras. Geociências* 7 (4), 349–364. doi:10.25249/0375-7536.1977349364

Awramik, S. M., and Margulis, L. (1974). "Definition of stromatolite," in *Stromatolite newsletter*. Editor E. Walter, 2, 5.

Awramik, S. M. (1992). "The history and significance of stromatolites," in *Early organic evolution* (Berlin, Heidelberg: Springer), 435–449.

Bartley, J. K., Knoll, A. H., Grotzinger, J. P., and Sergeev, V. N. (2000). "Lithification and fabric Genesis in precipitated stromatolites and associated peritidal carbonates, Mesoproterozoic Billi Akh Group, Siberia,". Editors J. P. Grotzinger and M. P. James (SEPM Spec. Publ.), 67, 59–73.*Carbonate Sediment. Diagenesis Evol. Precambrian World.*

Bertoni, M. E., Rooney, A. D., Selby, D., Alkmim, F. F., and Le Heron, D. P. (2014). Neoproterozoic Re–Os systematics of organic-rich rocks in the São Francisco Basin, Brazil and implications for hydrocarbon exploration. *Precambr. Res.* 255, 355–366. doi:10.1016/j.precamres.2014.10.010

Bertrand-Sarfati, J., and Moussine-Pouchkine, A. (1985). Evolution and environmental conditions of Conophyton—Jacutophyton associations in the atar dolomite (upper proterozoic, Mauritania). *Precambr. Res.* 29, 207–234. doi:10.1016/0301-9268(85)90069-5

Bertrand-Sarfati, J. (1972). Paléoécologie de certains stromatolites en récifs des formations du Précambrien supérieur du groupe d'Atar (mauritanie, sahara Occidental): création d'espèces nouvelles de ces récifs. *Palaeogeogr. Palaeoclimatol. Palaeoecol.* 11, 33–63.

Burne, R. V., and Moore, L. S. (1987). Microbialites: Organosedimentary deposits of benthic microbial communities. *Palaios* 2, 241. doi:10.2307/3514674

Burne, R. V. (2022). A radical reinterpretation of the growth and form of the stromatolite Conophyton lituus (Maslov) from evidence of syngenetic biofilm mineralisation. *J. Paleogeogr.*, 11, 69–84. doi:10.1016/j.jop.2021.09.003

Caird, R. A., Pufahl, P. K., Hiatt, E. E., Abram, M. B., Dourado, A. R., Kyser, T. K., et al. (2017). Ediacaran stromatolites and intertidal phosphorite of the Salitre Formation, Brazil: Phosphogenesis during the neoproterozoic oxygenation event. *Sediment. Geol.* 350, 55–71. doi:10.1016/j.sedgeo.2017.01.005

Chen, C., Hall, S. J., Coward, E., and Thompson, A. (2020). Iron-mediated organic matter decomposition in humid soils can counteract protection. *Nat. Commun.* 11, 2255. doi:10.1038/s41467-020-16071-5

Cloud, P., and Dardenne, M. (1973). Proterozoic age of the bambui group in Brazil. *Geol. Soc. Am. Bull.* 84, 1673–1676. doi:10.1130/0016-7606(1973)84<1673:PAOTBG>2.0.CO;2

Cloud, P., and Moeri, E. (1973). Conophyton in the bambui group: What form and age? *Geology* 1 (3), 127. doi:10.1130/0091-7613(1973)1<127:CITBGW>2.0.CO;2

Compton, J., Mallinson, D., Glenn, C. R., Filippelli, G., Föllmi, K., Shields, G., et al. (2000). "Variations in the global phosphorus cycle," in *Marine authigenesis: From global to microbial* (Tulsa, OK: Society of Economic Paleontologists and Mineralogists Special Publication), 66, 21–33. doi:10.2110/pec.00.66.0021

Crosby, C. H., and Bailey, J. V. (2012). The role of microbes in the formation of modern and ancient phosphatic mineral deposits. *Front. Microbiol.* 3, 241. doi:10.3389/fmicb.2012.00241

Dardenne, M. A., Mello, S. M. G., and Moeri, E. (1972). Conophyton: Um fóssil index do precambriano no grupo Bambuí. *Ciênc. Cult.* 24 (2), 199–203.

Dardenne, M. A. (2000). "The Brasília Fold belt," in Tectonic evolution of South America,31 international geological congress, Rio de Janeiro, Brazil. Editors U. G. Cordani, E. J. Milani, A. Thomaz Filho, and D. A. Campos, 231–264.

Dardenne, M. A. (2005). "Conophytons de Cabeludo, Grupo Vazante (MG) – registro de construções dolomíticas por cianobactérias no Proterozóico do Brasil," in *Sítios Geológicos e Paleontológicos do Brasil*. Editors M. Winge, A. C. S. Fernandes, C. Schobbenhaus, C. R. G. Souza, D. A. Campos, E. T. Queiroz, et al.

Davey, M. E., and O'Toole, G. A. (2000). Microbial biofilms: From ecology to molecular genetics. *Microbiol. Mol. Biol. Rev.* 64, 847–867. doi:10.1128/MMBR.64.4.847-867.2000

De Nolf, W., Vanmeert, F., and Janssens, K. (2014). XRDUA: crystalline phase distribution maps by two-dimensional scanning and tomographic (micro) X-ray powder diffraction. *J. Appl. Crystallogr.* 47, 1107–1117. doi:10.1107/S1600576714008218

Decho, A. W. (1999). "Chemical communication within microbial biofilms: chemotaxis and quorum sensing in bacteria cells," in *Microbial extracellular polymeric substances*. Editors J. Wingender, T. Neu, and H.-C. Flemming (Berlin: Springer), 155–169. doi:10.1007/978-3-642-60147-7_9

Des Marais, D. J. (1990). Microbial mats and the early evolution of life. *Trends Ecol. Evol.* 5, 140–144. doi:10.1016/0169-5347(90)90219-4

Dupraz, C., and Visscher, P. T. (2005). Microbial lithification in marine stromatolites and hypersaline mats. *Trends Microbiol.* 13, 429–438. doi:10.1016/j.tim.2005.07.008

Dupraz, C., Reid, R. P., Braissant, O., Decho, A. W., Norman, R. S., Visscher, P. T., et al. (2009). Processes of carbonate precipitation in modern microbial mats. *Earth-Science Rev.* 96, 141–162. doi:10.1016/j.earscirev.2008.10.005

Fairchild, T. R., Rohn, R., Dardenne, M. A., Alvarenga, C. J. S., and Guimarães, E. M. (2015). "Microbialitos dos Grupos Paranoá (Mesoproterozoico) e Vazante (Neoproterozoico), Distrito federal, Goiás e Minas Gerais," in *Microbialitos do brasil do pré-cambriano ao recente: um atlas. Rio claro*. Editors T. R. Fairchild, R. Rohn, and D. Dias-Brito (Obra: UNESP-IGCE-UnesPetro), 2, 90–151.

Falci, A., Caxito, F. A., Seer, H. J., Valeriano, C. M., Dias, P. H., Pedrosa-Soares, A. C., et al. (2018). Provenance shift from a continental margin to a syn-orogenic basin in the Neoproterozoic Araxá nappe system, southern Brasília belt, Brazil. *Precambrian Res.* 306, 209–219. doi:10.1016/j.precamres.2018.01.004

Ferris, F. G., Fratton, C. M., Gerits, J. P., Schultze-Lam, S., and Sherwood Lollar, B. (1995). Microbial precipitation of a strontium calcite phase at a groundwater discharge zone near rock Creek, British Columbia, Canada. *Geomicrobiol. J.* 13 (1), 57–67. doi:10.1080/01490459509378004

Foster, J. S., and Green, S. J. (2011). "Microbial diversity in modern stromatolites," in *Stromatolites: Interaction of microbes with sediments. Cellular origin, life in extreme habitats and astrobiology*. Editors V. Tewari and J. Seckbach (Dordrecht: Springer), 18. doi:10.1007/978-94-007-0397-1_17

Foster, J. S., and Mobberley, J. M. (2010). "Past, present, and future: microbial mats as models for astrobiological research," in *Cellular origin, life in extreme habitats and astrobiology: Microbial mats: Modern and ancient microorganisms in stratified systems*. Editors J. Seckbach and A. Oren (Springer), 563–582. doi:10.1007/978-90-481-3799-2_29

Gaft, M., Reisfeld, R., and Panczer, G. (2015). *Modern luminescence spectroscopy of minerals and materials*. Switzerland: Springer International Publishing, 606.

Gaucher, C., Cernuschi, F., and Chiglino, L. (2004). "Ocurrencia de Conophyton en Cantera Burgueño (Nueva Carrara, Uruguay): nuevos afloramientos del Grupo Mina Verdún y su importancia. IV Congreso Uruguayo de Geología," in *Cuarto congreso uruguayo de Geología, CD*.

Graf, D. L. (1961). Crystallographic tables for the rhombohedral carbonates. *Am. Mineral.* 46, 1283–1316.

Grotzinger, J. P. (1989). "Facies and evolution of precambrian depositional systems: emergence of the modern platform archetype," in *Controls on carbonate platform and basin development*. Editors P. D. Crevello, J. J. Wilson, J. F. Sarg, and J. F. Read (SEPM Spec. Pub.), 44, 79–106.

Habermann, D., Neuser, R. D., and Richter, D. K. (1998). Low limit of Mn2+-activated cathodoluminescence of calcite: state of the art. *Sediment. Geol.* 116, 13–24. doi:10.1016/S0037-0738(97)00118-8

Havemann, S. A., and Foster, J. S. (2008). Comparative characterization of the microbial diversities of an artificial microbialite model and a natural stromatolite. *Appl. Environ. Microbiol.* 74, 7410–7421. doi:10.1128/AEM.01710-08

Hickman-Lewis, K., Cavalazzi, B., Sorieul, S., Gautret, P., Foucher, F., Whitehouse, J. M., et al. (2020). Metallomics in deep time and the influence of ocean chemistry on the metabolic landscapes of Earth's earliest ecosystems. *Sci. Rep.* 10, 4965. doi:10.1038/s41598-020-61774-w

Hoffman, P. F. (1976). "Environmental diversity of middle precambrian stromatolites," in *Stromatolites*. Editor M. R. Walter (Amsterdam: Elsevier), 599–611.

Hofmann, H. J. (1969). Attributes of stromatolites. *Geol. Surv. Can. Pap.* 58, 69–39.

Hofmann, H. J. (2000). "Archean stromatolites as microbial archives," in *Microbial sediments*. Editors R. Riding and S. Awramik (Berlin, Heidelberg: Springer), 315–327.

Horodyski, R. J. (1985). "Stromatolites of the middle proterozoic belt Supergroup, glacier national park, Montana: a summary and a comment on the relationship between their morphology and paleoenvironment," in *Paleoalgology*. Editors D. F. Toomey and M. H. Nitecki (Berlin, Heidelberg: Springer). doi:10.1007/978-3-642-70355-3_4

Kah, L. C., Bartley, J. K., and Stagner, A. F. (2009). "Reinterpreting a proterozoic enigma: Conophyton–Jacutophyton stromatolites of the mesoproterozoic atar

group, Mauritania" in *Perspectives in Carbonate Geology, A Tribute to the Career of Robert Nathan Ginsburg*, 41. Chichester, Wiley: International Association of Sedimentologists Spec. Publ., 277–295.

Kögel-Knabner, I., Guggenberger, G., Kleber, M., Kandeler, E., Kalbitz, K., Scheu, S., et al. (2008). Organo-mineral associations in temperate soils: Integrating biology, mineralogy, and organic matter chemistry. *Z. Pflanzenernahr. Bodenk.*, 171, 61–82. doi:10.1002/jpln.200700048

Lalonde, K., Mucci, A., Ouellet, A., and Gélinas, Y. (2012). Preservation of organic matter in sediments promoted by iron. *Nature* 483, 198–200. doi:10.1038/nature10855

Lovley, D. R., Coates, J. D., Blunt-Harris, E. L., Phillips, E. J. P., and Woodward, J. C. (1996). Humic substances as electron acceptors for microbial respiration. *Nature* 382, 445–448. doi:10.1038/382445a0

MacRae, C., and Wilson, N. (2008). Luminescence database I—minerals and materials. *Microsc. Microanal.*, 14 (2), 184–204. doi:10.1017/S143192760808029X

Marfunin, A. S. (1995). *Methods and instrumentations: Results and recent developments*. Berlin Heidelberg: Springer-Verlag, 441p.

Melim, L. A., Northup, D. E., Boston, P. J., and Spilde, M. N. (2016). Preservation of fossil microbes and biofilm in cave pool carbonates and comparison to other microbial carbonate environments. *Palaios* 31 (4), 177–189. doi:10.2110/palo.2015.033

Moeri, E. (1972). On a columnar stromatolite in the precambrian bambui group of central Brazil. *Eclogae Geol. Helv.* 65 (1), 185–195. doi:10.5169/seals-164084

Murphy, A. E., Wieman, S. T., Gross, J., Stern, J. C., Steele, A., Glamoclija, M., et al. (2020). Preservation of organic carbon in dolomitized Cambrian stromatolites and implications for microbial biosignatures in diagenetically replaced carbonate rock. *Sediment. Geol.* 410, 105777. doi:10.1016/j.sedgeo.2020.105777

Neu, T. R. (1994). "Biofilms and microbial mats," in *Biostabilization of sediments*. Editors W. E. Krumbein, D. M. Paterson, and L. Stal (Oldenburg: BIS-Verlag), 6–16.

Neu, T. R. (1996). Significance of bacterial surface-active compounds in interaction of bacteria with interfaces. *Microbiol. Rev.* 60, 151–166. doi:10.1128/mr.60.1.151-166.1996

Nielsen, L. P., Risgaard-Petersen, N., Fossing, H., Christensen, P. B., and Sayama, M. (2010). Electric currents couple spatially separated biogeochemical processes in marine sediment. *Nature* 463, 1071–1074. doi:10.1038/nature08790

Nisbet, E. G., and Fowler, C. M. R. (1999). Archaean metabolic evolution of microbial mats. *Proc. R. Soc. Lond. B* 266, 2375–2382. doi:10.1098/rspb.1999.0934

Noffke, N., and Awramik, S. M. (2013). Stromatolites and MISS – differences between relatives. *GSA Today* 23, 4–9. doi:10.1130/GSATG187A.1

Noffke, N., Christian, D., Wacey, D., and Hazen, R. M. (2013). Microbially induced sedimentary structures recording an ancient ecosystem in the. ca. 3.48 billion-year-old Dresser Formation, Pilbara, Western Australia. *Astrobiology* 13 (12), 1103–1124. doi:10.1089/ast.2013.1030

Pernthaler, A., Dekas, A. E., Brown, T., Goffredi, S. K., Embaye, T., Orphan, V. J., et al. (2008). Diverse Syntrophic partnerships from deep-sea methane vents revealed by direct cell capture and metagenomics. *Proc. Natl. Acad. Sci. U. S. A.*, 105 7052–7057. doi:10.1073/pnas.0711303105

Pierson, B. J. (1981). The control of cathodoluminescence in dolomite by iron and manganese. *Sedimentology* 28, 601–610. doi:10.1111/j.1365-3091.1981.tb01924.x

Preiss, W. V. (1976). "Intercontinental correlations," in *Stromatolites*. Editor M. R. Walter (Amsterdam: Elsevier Sci. Publ. Co.), 359–370.

Reid, R. P., and MacIntyre, I. G. (2000). Microboring versus recrystallization: further insight into the micritization process. *J. Sediment. Res.* 70, 24–28. doi:10.1306/2DC408FA-0E47-11D7-8643000102C1865D

Riding, R. (2011). "The nature of stromatolites: 3,500 million years of history and a century of research," in *Advances in stromatolite geobiology* (Berlin, Heidelberg: Springer), 131. Lecture notes in Earth sciences. doi:10.1007/978-3-642-10415-2_3

Rodrigues, J. B., Pimentel, M. M., Bühn, B., Matteini, M., Dardenne, M. A., Alvarenga, C. J. S., et al. (2012). Provenance of the Vazante group: New U–Pb, Sm–Nd, Lu–Hf isotopic data and implications for the tectonic evolution of the neoproterozoic Brasília belt. *Gondwana Res.* 21 (2- 3), 439–450. doi:10.1016/j.gr.2011.07.017

Saghaï, A., Gutiérrez-Preciado, A., Deschamps, P., Moreira, D., Bertolino, P., Ragon, et al. (2017). Unveiling microbial interactions in stratified mat communities from a warm saline shallow pond. *Environ. Microbiol.* 19 (6), 2405–2421. doi:10.1111/1462-2920.13754

Sallun Filho, W., and Fairchild, T. R. (2005). *Estudo comparativo entre estromatólitos do tipo Conophyton das Faixas Ribeira e Brasília*. São Paulo: Revista do Instituto Geológico, 1–18. doi:10.5935/0100-929X.20050001

Schopf, J. W. (1975). Precambrian paleobiology: problems and perspectives. *Annu. Rev. Earth Planet. Sci.* 3, 213–249. doi:10.1146/annurev.ea.03.050175.001241

Schopf, J. W., and Yuk, S. (1976. Microfossils in conophyton from the vendian deposits of South Kazakhstan. *Doklady AN SSSR* 230, 1448–1450. (In Russian)

Schulz, H. N., and Schulz, H. D. (2005). Large sulfur bacteria and the formation of phosphorite. *Science* 307, 416–418. doi:10.1126/science.1103096

Shionoya, S., Yen, W. M., and Yamamoto, H. (2007). *Phosphor handbook*. 2nd ed.. Boca Raton, FL: CRC Press/Taylor and Francis, 1080. doi:10.1201/9781315222066

Shukla, Y., Sharma, M., Noffke, N., and Callefo, F. (2020). Biofilm microfacies in phosphoritic units of the neoproterozoic halkal shale, bhima basin, South India. *Precambr. Res.* 349, 105501. doi:10.1016/j.precamres.2019.105501

Solé, V. A., Papillon, E., Cotte, M., Walter, P., and Susini, J. (2007). A multiplatform code for the analysis of energy-dispersive X-ray fluorescence spectra. *Spectrochim. Acta Part B At. Spectrosc.* 62, 63–68. doi:10.1016/j.sab.2006.12.002

Stolyar, S., Dien, S. V., Hillesland, K. L., Pinel, N., Lie, T. J., Leigh, J. A., et al. (2007). Metabolic modeling of a mutualistic microbial community. *Mol. Syst. Biol.* 3, 92. doi:10.1038/msb4100131

Stoodley, P., Sauer, K., Davies, D. G., and Costerton, J. W. (2002). Biofilms as complex differentiated communities. *Annu. Rev. Microbiol.* 56, 187–209. doi:10.1146/annurev.micro.56.012302.160705

Tolentino, H. C. N., Geraldes, R. R., Moreno, G. B. Z. L., Pinto, A. C., Bueno, C. S. N. C., Kofukuda, L. M., et al. (2021). "X-ray microscopy developments at sirius-LNLS: first commissioning experiments at the Carnauba beamline," in Proceedings SPIE 11839, X-Ray Nanoimaging: Instruments and Methods V, 8 September 2021. doi:10.1117/12.259649*61183904*

Tolker-Nielsen, T., and Molin, S. (2000). Spatial organization of microbial biofilm communities. *Microb. Ecol.* 40, 75–84. doi:10.1007/s002480000057

Vasconcelos, A. G., Bittencourt, J. S., Eliziário, N. F., Kraemer, B. M., and Auler, A. S. (2020). Stromatolites in caves in southeastern Brazil and their importance to geoconservation. *Geoheritage* 12, 48. doi:10.1007/s12371-020-00469-0

Walter, M. R. (1976). *Stromatolites*. Amsterdam: Elsevier Sci. Publ. Co., 790.

Walter, M. R. (1977). Interpreting Stromatolites: These fossils can tell us much about past organisms and environments if we can learn to decode their message. *Am. Sci.* 65 (5), 563–571. Available at: http://www.jstor.org/stable/27848083.

Williams, L. A., and Reimers, C. (1983). Role of bacterial mats in oxygen-deficient marine basins and coastal upwelling regimes: preliminary report. *Geology* 11, 267–269. doi:10.1130/0091-7613(1983)11<267:ROBMIO>2.0.CO;2

Williams, L. A. (1984). Subtidal stromatolites in monterey formation and other organic-rich rocks as suggested source contributors to petroleum formation. *Am. Assoc. Pet. Geol. Bull.* 68, 1879–1893. doi:10.1306/AD4619F8-16F7-11D7-8645000102C1865D

Zhang, Y., Li, J., Chen, L., Wei, Y., Shi, Q., Wang, D. G., et al. (2021). Manganese carbonate stromatolites of the ediacaran doushantuo formation in chengkou, northern yangtze Craton, China. *J. Palaeogeogr.* 10, 22. doi:10.1186/s42501-021-00099-9